

Supporting Information:

Racemized Photonic Crystals for Physical Unclonable Function

*Geonhyeong Park,^{†,a} Hyewon Park,^{†,a} Joanna M. Wolska,^b Jesse Gaehyun Park,^a and Dong
Ki Yoon^{a,c,*}*

^a Department of Chemistry, Korea Advanced Institute of Science and Technology, Daejeon
34141, Republic of Korea

^b Faculty of Chemistry, University of Warsaw, Warsaw 02-093, Poland

^c KAIST Institute for Nanocentury, Korea Advanced Institute of Science and Technology,
Daejeon 34141, Republic of Korea

[†]These authors contributed equally.

*To whom correspondence should be addressed.

E-mail: nandk@kaist.ac.kr

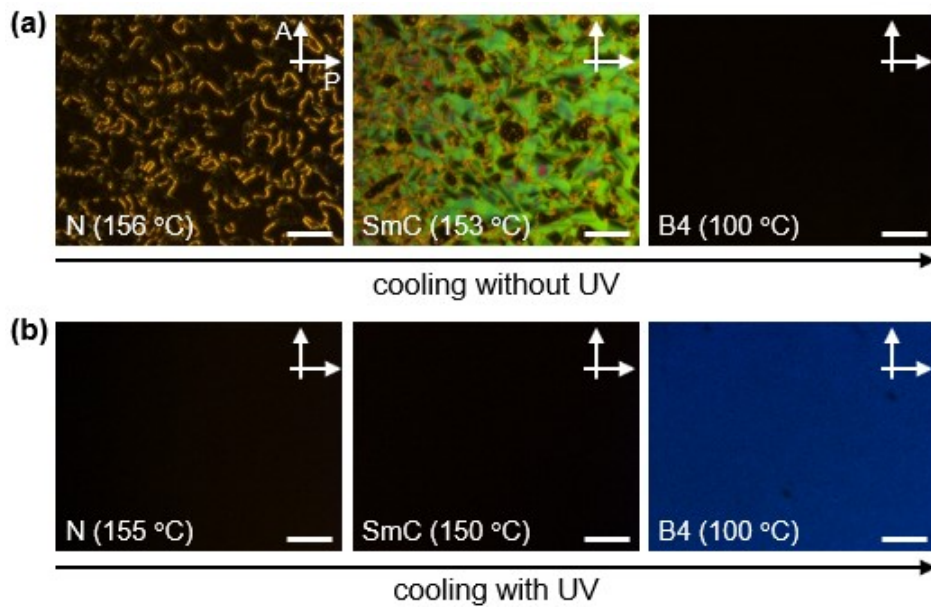


Fig. S1 POM images of azobenzene dimers during the phase transition (a) without UV irradiation and (b) with UV irradiation. Scale bars are 50 μm .

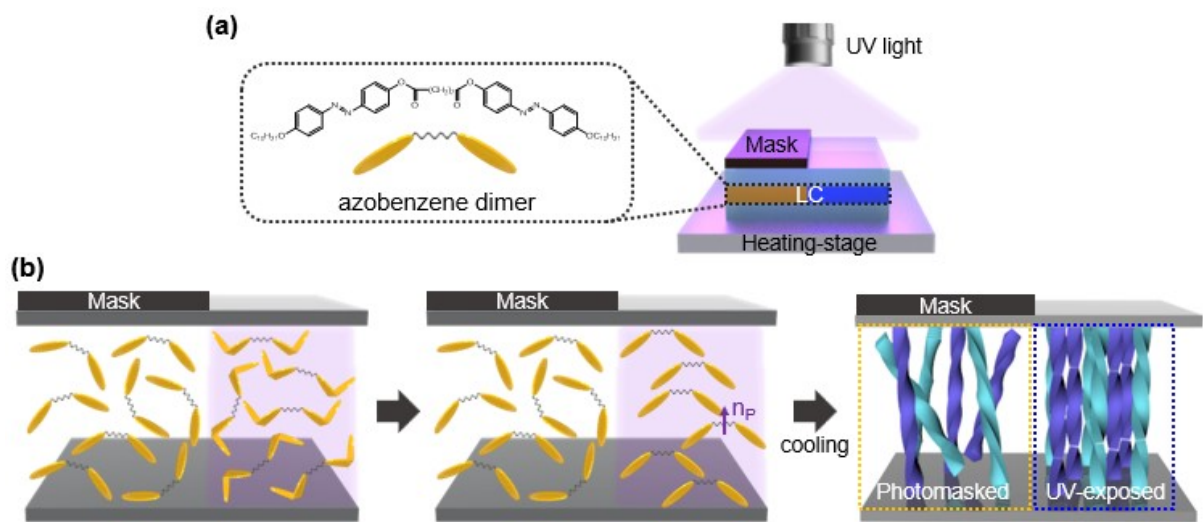


Fig. S2 Light-driven orientation of HNFs. (a) Schematic illustration of the fabrication method for HNF photonic crystal (PC) with azobenzene dimer. (b) Photoisomerization process of azobenzene dimer depending on UV exposure and the resulting HNFs after the phase transition process. n_p represents the polar director of dimeric molecules.

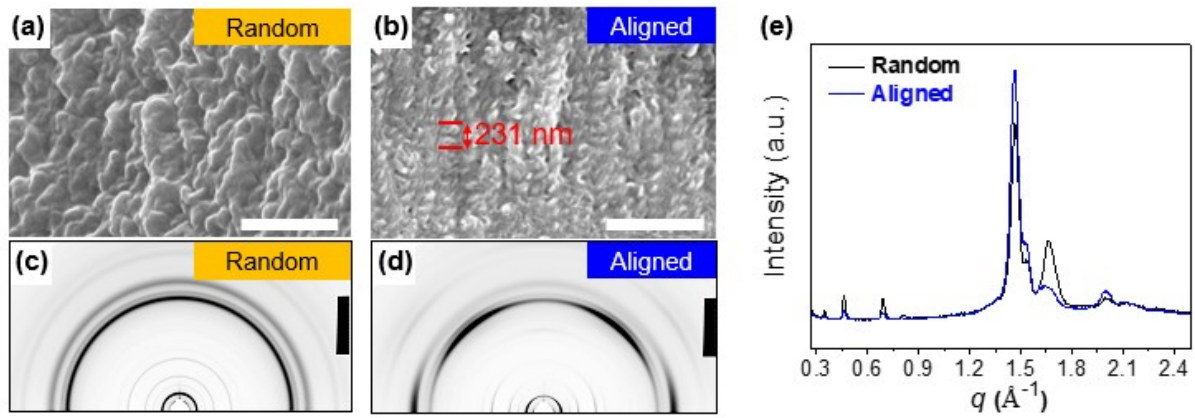


Fig. S3 Structural analysis of HNFs. Scanning electron microscopic (SEM) images and 2D grazing incidence X-ray diffraction (GIXD) images of (a,c) masked and (b,d) UV-exposed regions, respectively. The helical pitch of photo-aligned HNF is ~ 231 nm. (e) 1D plotted GIXD results. Scale bars are (a) 500 nm and (b) 1 μm .

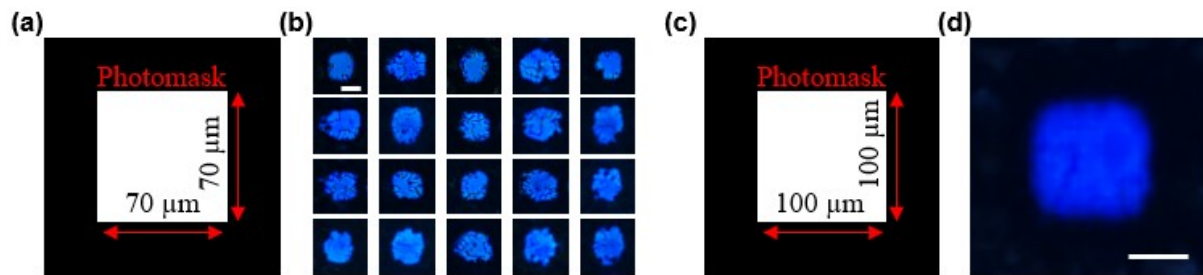


Fig. S4 Shape variation of the PCs according to the dimension of the photomask. Photomask images with the square shape of dimensions (a) 70 μm and (c) 100 μm . (b) POM images at $\theta = 90^\circ$ for the non-standardized PC patterns with the photomask dimension below the diffraction limit. (d) A POM image at $\theta = 90^\circ$ for the regular PC pattern with the photomask dimension above the diffraction limit. Scale bar is 50 μm .

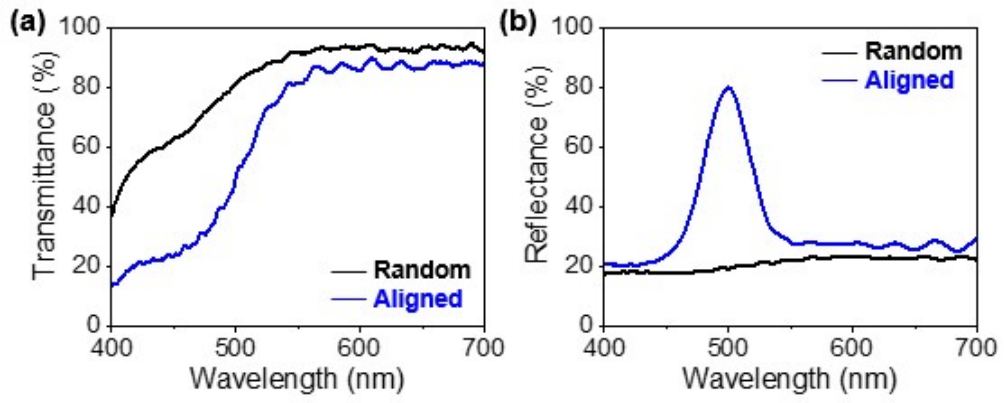


Fig. S5 (a) Transmittance and (b) reflectance spectra of randomly oriented and photo-aligned HNFs, respectively.

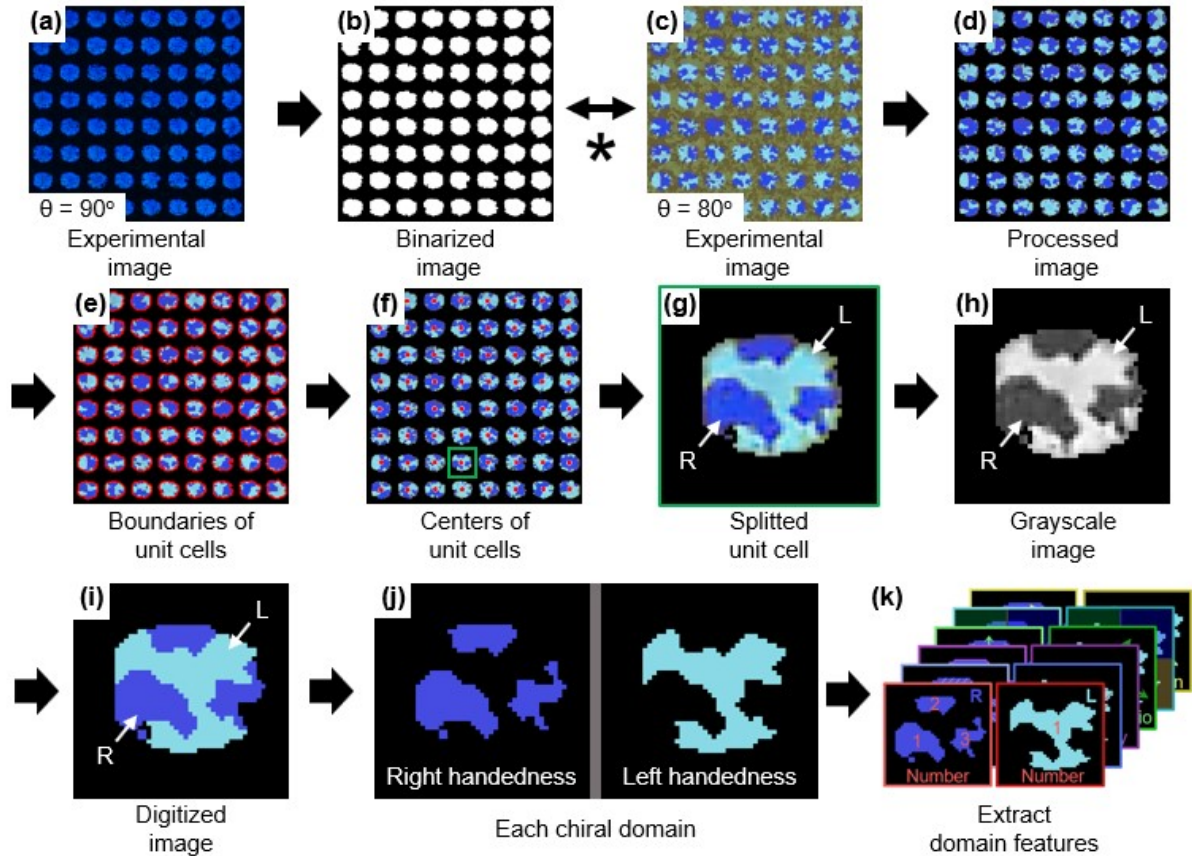


Fig. S6 A sequential digitization process of POM images to extract morphological features. Experimental POM image at (a) $\theta = 90^\circ$ and (c) $\theta = 80^\circ$ of patterned PCs, where $N = 64$. (b) A binarized image by distinguishing the patterned PC areas in (a). (d) An image obtained through the “AND” operation of (b) and (c). (e) After setting the boundaries of the patterned PC areas, (f) the centers of each unit cell were defined. (g) The processed image was divided into the unit cell images of the finite size (47×47 pixels) and, (h) converted to grayscale. (i) The images were binarized according to the chirality of domains. (j) Lastly, each domain was deconvoluted. The black areas in (d-j) were considered virtual. (k) Extraction of the six morphological features, including the number of chiral domains, area, circularity, aspect ratio, position and orientation, of each chiral domain.

Note: All image processing used homemade MATLAB codes. First, the experimental POM image at $\theta = 90^\circ$ (Fig. S6a) was divided into the blue areas and the dark areas based on RGB coordinates. The image noises were eliminated using “bwareaopen” and “imfill” functions, and the processed images were binarized into the PC regions and the non-PC region (Fig. S6b). And then, a processed image (Fig. S6d) is obtained through “AND” operation of the POM image of $\theta = 80^\circ$ (Fig. S6c) and the binarized image (Fig. S6b). “bwboundaries” function was

applied to the processed image to define the boundaries of the unit cells (Fig. S6e) and obtained the centroid coordinates (red dots) of each patterned PC (Fig. S6f). Based on this center coordinate, the processed image was divided into the unit cell images with defined size, 47×47 pixels (Fig. S6g). Here, the black regions are considered virtual. After the colored regions were converted to grayscale (Fig. S6h), the image was binarized to “0” for right-handed and “1” for left-handed chiral domains (Fig. S6i). The digitized chiral domains were deconvoluted into the two images (Fig. S6j), and their morphological features were extracted through the “regionsprop” function (Fig. S6k). The number and area of each chiral domain were obtained using “Area” variable of this function. The circularity of domains was calculated using the “Circularity” variable. The aspect ratio could be obtained through the “MajorAxisLength” and “MinorAxisLength” variables, and the orientation angle of the domains was achieved using the “Orientation” variable. The position of the domains was defined as the angle between the center of the domain derived with “Centroid” variable and the center of the 47×47 pixels image. Morphological features extracted from the right or left chiral domains were converted in the form of 6×6 matrices and stored in the database as $6 \times 6 \times 2$ matrix. An image containing N unit cells were stored in the database as $6 \times 6 \times 2 \times N$ matrix.

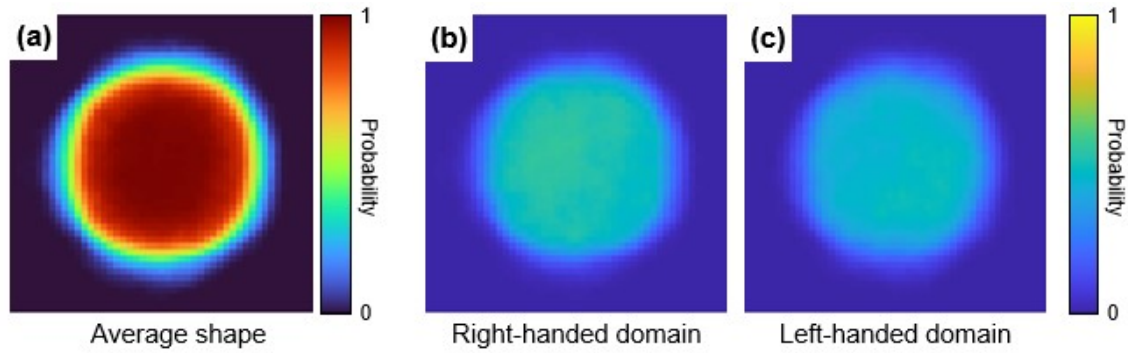


Fig. S7 Average shape of patterned PC and frequency of chiral domains in a unit cell. (a) A heatmap for the average shape of HNF PCs when using a $70\ \mu\text{m}$ square photomask. Heatmaps for the frequencies of the (b) right and (c) left-handed domains in a unit cell. All heatmaps are obtained by comparing the 960 unit cell images.

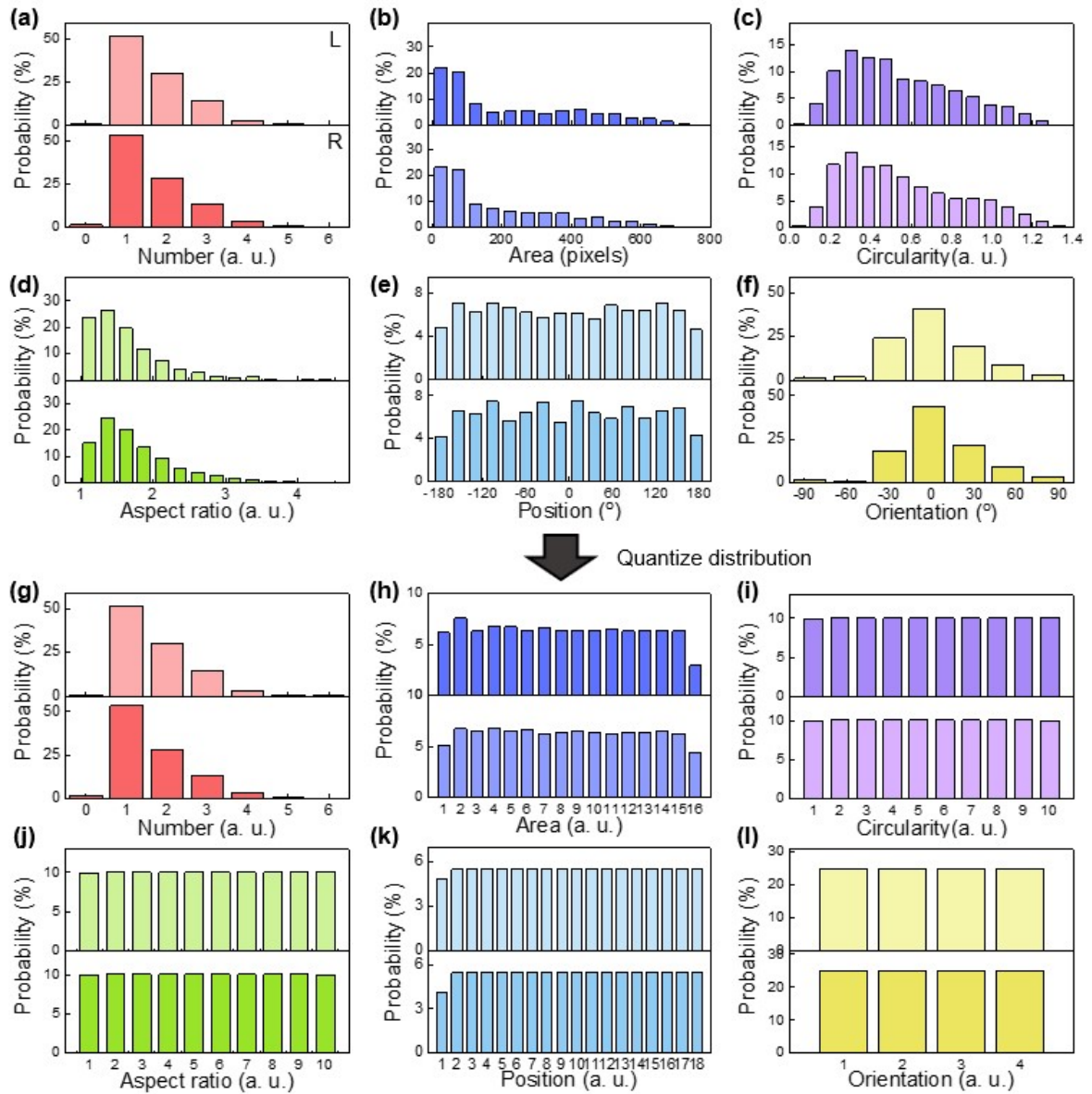


Fig. S8 Distribution of the morphological features extracted from chiral domains. Raw distributions of morphological features, including (a) the number of chiral domains, (b) area, (c) circularity, (d) aspect ratio, (e) position and (f) orientation. The data were extracted from 960 unit cell images. The top and bottom distributions in a graph represent the right and left-handed chiral domain properties, respectively. (g-l) Continuous distributions, except the number of domains, are quantized by introducing appropriate class levels.

Table S1. The upper limit and the lower limit of the classes according to the morphological features for right-handed domains.

Levels	Area (pixels) Right	Cir. (a. u.) Right	Asp. (a. u.) Right	Pos. (°) Right	Ori. (°) Right
1	0 ~ 34	0.00 ~ 0.22	0.00 ~ 1.16	0.00 ~ 23.16	0.00 ~ 90.74
2	35 ~ 39	0.23 ~ 0.29	1.17 ~ 1.25	23.17 ~ 39.28	90.75 ~ 176.7
3	40 ~ 46	0.3 ~ 0.35	1.26 ~ 1.35	39.29 ~ 57.67	176.71 ~ 266.94
4	47 ~ 54	0.36 ~ 0.42	1.36 ~ 1.47	57.68 ~ 78.53	> 266.94
5	55 ~ 66	0.43 ~ 0.49	1.48 ~ 1.58	78.54 ~ 98.64	
6	67 ~ 84	0.5 ~ 0.58	1.59 ~ 1.7	98.65 ~ 111.34	
7	85 ~ 110	0.59 ~ 0.69	1.71 ~ 1.87	111.35 ~ 129.95	
8	111 ~ 155	0.7 ~ 0.8	1.88 ~ 2.11	129.96 ~ 147.53	
9	156 ~ 216	0.81 ~ 0.95	2.12 ~ 2.55	147.54 ~ 181.15	
10	217 ~ 270	> 0.95	> 2.55	181.16 ~ 218.27	
11	271 ~ 332			218.28 ~ 252.35	
12	333 ~ 394			252.36 ~ 275.23	
13	395 ~ 447			275.24 ~ 289.09	
14	448 ~ 516			289.1 ~ 301.57	
15	517 ~ 602			301.58 ~ 311.63	
16	> 602			311.64 ~ 325.35	
17				325.36 ~ 342.72	
18				> 342.72	

Table S2. The upper limit and the lower limit of the classes according to the morphological features for left-handed domains.

Levels	Area (pixels) Left	Cir. (a. u.) Left	Asp. (a. u.) Left	Pos. (°) Left	Ori. (°) Left
1	0 ~ 34	0.00 ~ 0.27	0.00 ~ 1.19	0.00 ~ 20.59	0.00 ~ 89.88
2	35 ~ 40	0.28 ~ 0.33	1.2 ~ 1.3	20.6 ~ 37.84	89.99 ~ 184.2
3	41 ~ 47	0.34 ~ 0.39	1.31 ~ 1.4	37.85 ~ 55.36	184.21 ~ 271.88
4	48 ~ 56	0.4 ~ 0.46	1.41 ~ 1.5	55.37 ~ 81.86	> 271.88
5	57 ~ 66	0.47 ~ 0.53	1.51 ~ 1.62	81.87 ~ 100.64	
6	67 ~ 82	0.54 ~ 0.6	1.63 ~ 1.75	100.65 ~ 115.24	
7	83 ~ 106	0.61 ~ 0.71	1.76 ~ 1.91	115.25 ~ 131.07	
8	107 ~ 144	0.72 ~ 0.85	1.92 ~ 2.15	131.08 ~ 153.06	
9	145 ~ 177	0.86 ~ 0.99	2.16 ~ 2.54	153.07 ~ 186.63	
10	178 ~ 227	> 0.99	> 2.55	186.64 ~ 221.91	
11	228 ~ 283			221.92 ~ 251.43	
12	284 ~ 338			251.44 ~ 275.41	
13	339 ~ 393			275.42 ~ 290.28	
14	394 ~ 474			290.29 ~ 301.92	
15	475 ~ 598			301.93 ~ 312.36	
16	> 599			312.37 ~ 326.63	
17				326.64 ~ 340.6	
18				> 340.6	

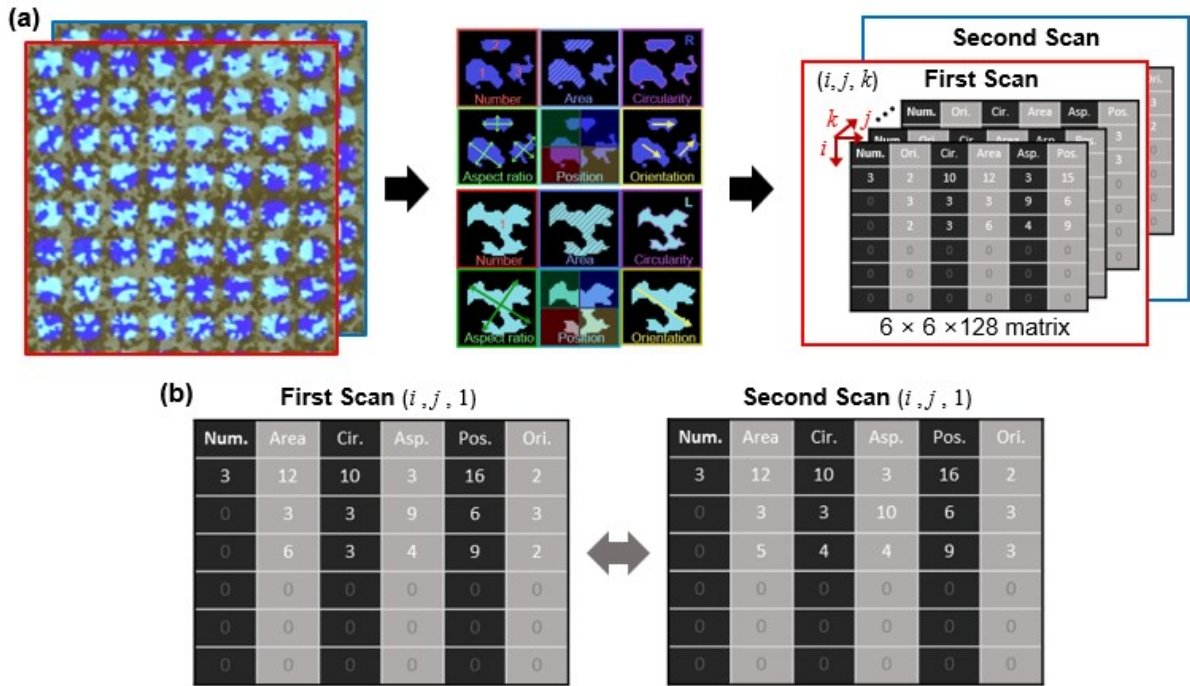


Fig. S9 A schematic diagram of obtaining matrix data from experimental images and an example of obtaining similarity indices (S_f) through pairwise comparison. (a) Two $6 \times 6 \times 128$ matrices data are generated by scanning samples ($N = 64$) twice. (b) An example to show how to calculate S_f by comparing the obtained 128 two-dimensional matrices.

Note: The similarity indices (S_f) for each feature (f), including area, circularity, aspect ratio, position and orientation, were calculated to evaluate misrecognition rate (MRR) and apply it to the validation process. The digitized matrices extracted by scanning the experimental image twice went through pairwise comparison to get S_f of the same chiral PUFs and those of different ones. Samples composed of N unit cells generated $6 \times 6 \times 2 \times N$ matrix data. The matrix contained information about both the right and left-handed chiral domains. In the form of a 4D matrix, the 3D term represents chirality, where the first represents right-handedness and the second represents left-handedness. The 4D matrix ($6 \times 6 \times 2 \times N$) was transformed into a 3D matrix ($6 \times 6 \times 2N$) to calculate the similarity index. When the third term of the 3D matrix is referred as k , $1 \leq k \leq N$ and $N + 1 \leq k \leq 2N$ contained the morphological features for the right and left-handed chiral domains, respectively. Both matrices were calculated in the same way. 2D matrices with the same k were compared in each matrix from the two scans. First, the number of domains at $(1, 1, k)$ should be checked. If the two matrices have different values, the larger value is taken; otherwise, the same value is adopted. This value is defined as $M(k)$. After that, the other components were compared. In detail, each morphological feature

classified according to the second term (j) of matrix data was compared with the form of $M(k) \times 1$ to get the probability (P_f) for how many elements are equal in the same coordinates. In the case of Fig. S9b, where $M(1) = 3$, the P_f is calculated as follows; $P_{area} = 2/3$, $P_{cir.} = 2/3$, $P_{asp.} = 2/3$, $P_{pos.} = 1$, and $P_{ori.} = 2/3$. With this method, S_f , representing the similarity of each morphological feature, is defined as

$$I_f(R) = \sum_1^N \frac{P_f}{N} \quad (4)$$

$$I_f(L) = \sum_{N+1}^{2N} \frac{P_f}{N} \quad (5)$$

$$S_f = \log_{10} (I_f(R)I_f(L) + 1) \quad (6)$$

, where $I(R$ or $L)$ indicates the average of the probabilities of containing the same bits of each feature in right or left-handed domains. The calculated S_f has a maximum value of 0.301. The lower the value, the lower the similarity between the two samples.

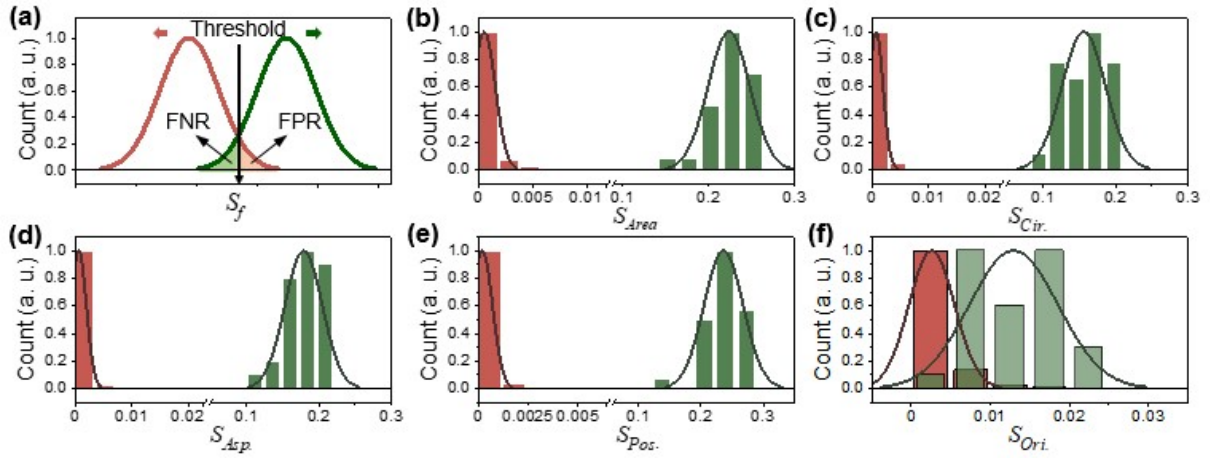


Fig. S10 Evaluation of false-negative rate (FNR) and false-positive rate (FPR) with similarity index (S_f). (a) Schematic diagram of how to calculate FNR, FPR, and threshold from the histograms of similarity indices. Histogram obtained by comparing digitized information for (b) area, (c) circularity, (d) aspect ratio, (e) position, and (f) orientation. The green graphs represent the S_f obtained by comparing identical samples, and the red graphs represent the S_f obtained by comparing different ones. All histograms are normalized to their maximums, and line graphs are obtained through the Gaussian fitting of each graph. These histograms are obtained by comparing 30 samples with $N = 64$.

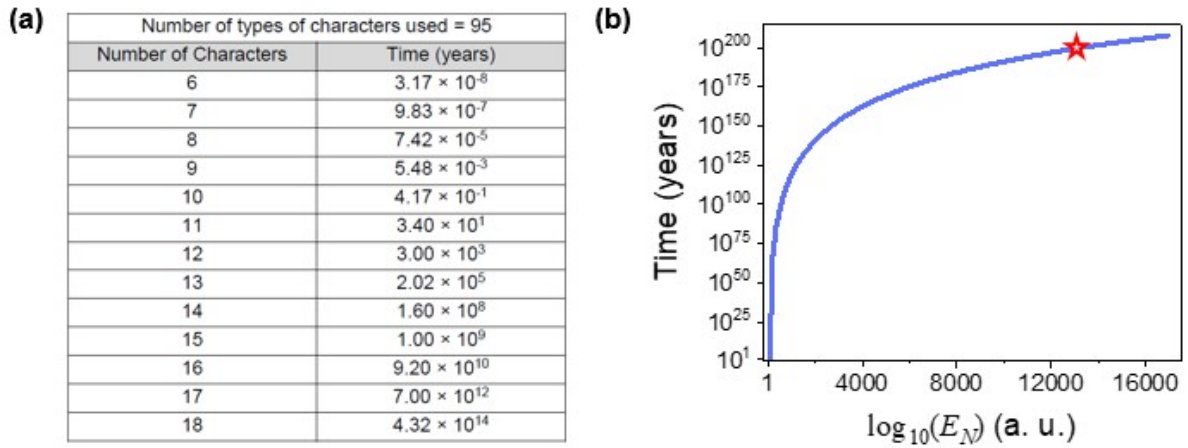


Fig. S11 The times required breaking the authentication systems via brute force attack. (a) Times required to break the security with a brute force attack through eight A100s (GPU, NVIDIA) against an authentication system composed of 95 types of characters. This table is open source data of *Hivesystem*. (b) Times needed to break security systems according to the encoding capacity (E_N) in the same attack environment. The red star indicates that a brute force attack takes $\sim 10^{199}$ years for $E_{256} = \sim 10^{13,000}$.

Note: The table is based on the data publicly provided by *Hivesystem* in 2022. It represents the time taken to hack the authentication systems with eight (GPU, NVIDIA) through the brute force algorithm according to the number of cases of the security key through. A graph of the time taken for a brute force attack according to the encoding capacity was obtained by fitting from a table at Fig. S11. In this table, encoding capacity can be regarded as 95^{NC} , where NC represent the number of characters. We fit this table with $\text{Time} = aX^b$, where $X = 95^{NC}$. With fitting, we got 1.26×10^{76} and 72.1 as the values of constants a and b . By replacing X with E_N , encoding capacity for chiral PUF containing N unit cells, we estimated the time required to hack the security system of the chiral PUF with a brute force attack. When $E_{256} = \sim 10^{13,000}$ the times for brute force attacks are estimated to be $\sim 10^{199}$ years.

Table S3. Thresholds for each step in the hierarchical verification algorithms.

	$T_{ori.}$	$T_{cir.}$	$T_{asp.}$	$T_{area.}$	$T_{pos.}$
Values	0.00300	0.00033	0.00028	0.00037	0.00530

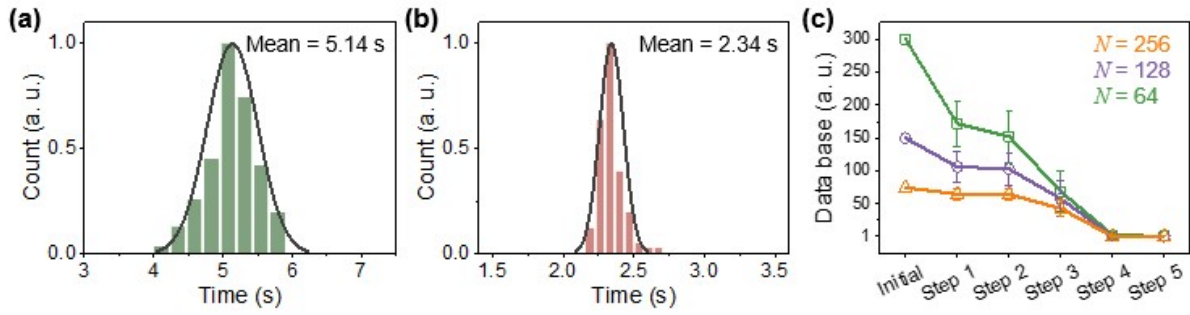


Fig. S12 Evaluation of processing speed in hierarchical verification method. Histograms of the processing speed for (a) genuine and (b) fake samples in the hierarchical verification method. The times are calculated over 100 genuine and 50 fake samples with $N = 64$, and the database is composed of 300 data points. (c) A graph showing the amount of database decreasing step by step in hierarchical verification. When $N = 256, 128,$ and 64 , the databases contains 300, 150, and 75 points. In addition, 100, 75, and 50 genuine samples are adopted for each evaluation. Error bars are defined as twice the standard deviation at each point.

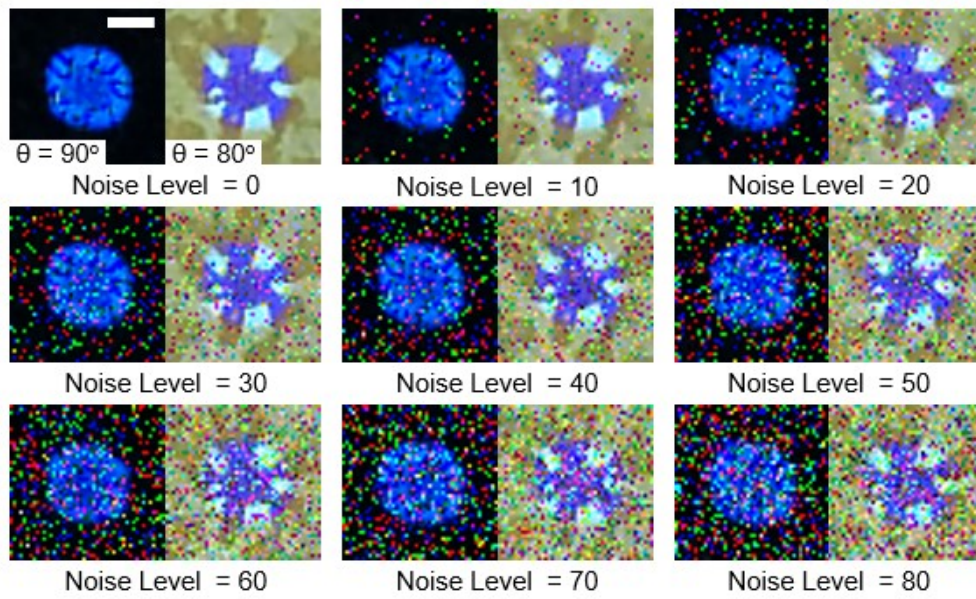


Fig. S13 Images with artificial noise applied to the original experimental ones. Noises are applied from 0 to 80 levels using the “salt & pepper” model. Scale bar is 50 μm .

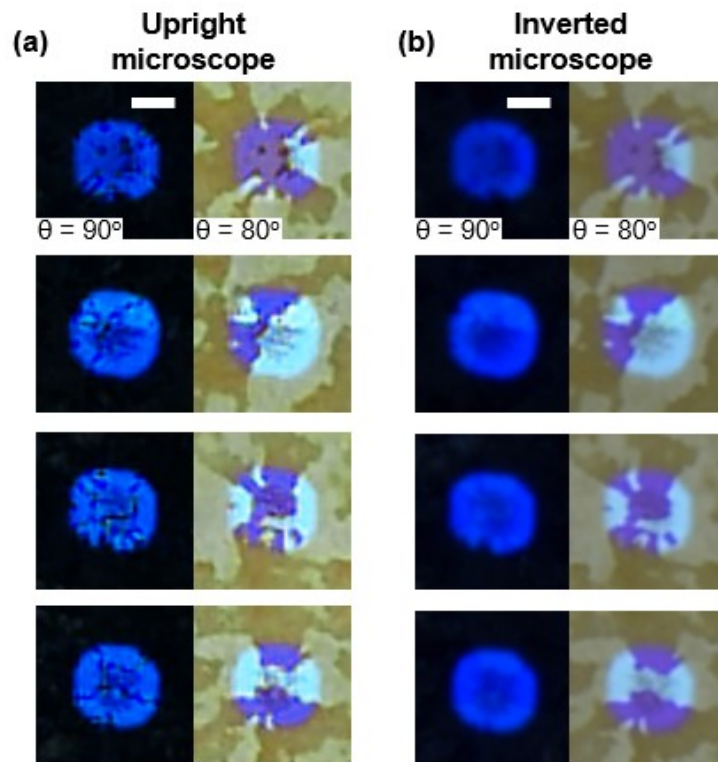


Fig. S14 Images of the same sample taken from two different POMs. (a) The POM images in the left columns are achieved with the upright POM and (b) the POM images in the right columns are achieved with the inverted POM. Scale bar is 50 μm .

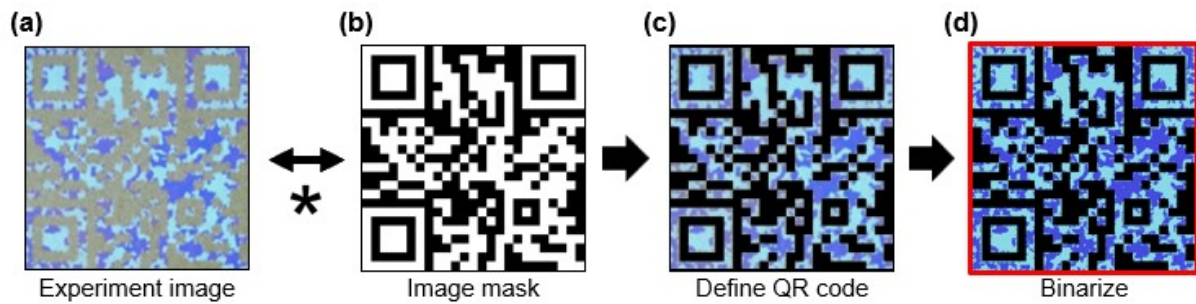


Fig. S15 A sequential image digitization process for a QR code embedding a chiral PUF. (a) An experimental POM image at $\theta = 80^\circ$ of HNF films patterned with a QR code. (b) A binarized image of predetermined QR code patterns. (c) An image obtained through the “AND” operation of (a) and (b). The black regions are considered virtual. (d) The remaining colored regions are converted to grayscale and binarized according to the chirality of the domains.

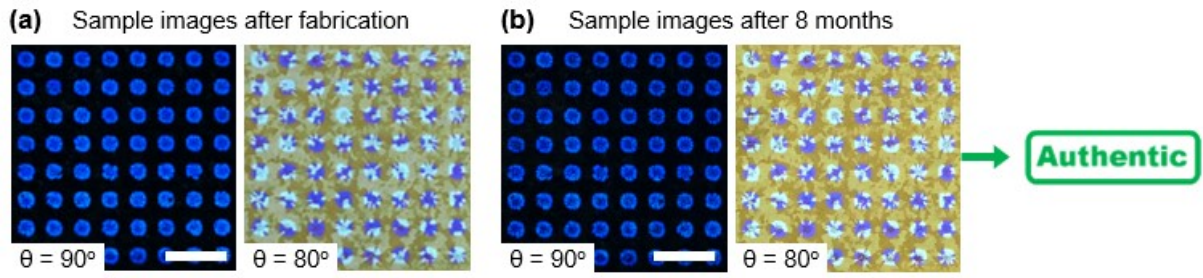


Fig. S16 POM images of HNF PC film taken over time. Experimental POM images of the patterned HNF PCs. The images were (a) captured immediately after fabrication or (b) 8 months after fabrication. Scale bars are 300 μm .